ACS OMEGA

Open Access

http://pubs.acs.org/journal/acsodf

Article

Reusable Wrinkled Nanoporous Silver Film Fabricated by Plasma Treatment for Surface-Enhanced Raman Scattering Applications

Published as part of ACS Omega virtual special issue "Celebrating 50 Years of Surface Enhanced Spectroscopy".

Jin-Hyun Ham, Jung Su Park, Myoung-Kyu Oh,* and Joon Heon Kim*

Cite This: *ACS Omega* 2023, 8, 47146−47152

Read Online

ACCESS | Metrics & More | Article Recommendations | Supporting Information

ABSTRACT: A nanoporous silver film (npAgF), a promising structure for surface-enhanced Raman spectroscopy (SERS), can be fabricated by using successive O_2 and Ar plasma treatments on a planar silver film. The common dealloying method for producing an npAgF involves annealing at high temperatures to produce an alloy film, as well as harsh etching using corrosive chemicals. By contrast, the plasma-based method can be applied directly to various functional substrates to produce more sophisticated npAgF structures. Herein, we report a facile fabrication method for a wrinkled npAgF (w-npAgF) for SERS applications using a thermally contractible polystyrene substrate. The w-npAgF had 3D wrinkles of the nanoporous structure and showed approximately 8 times higher SERS enhancement than did the flat npAgF. Moreover, the w-npAgF could be reused for multiple SERS measurements of different molecules by mild O_2 and Ar plasma treatments after each use, in which the O_2 plasma effectively removed the adsorbed organic molecules and the Ar plasma reduced silver oxide to pristine silver for subsequent SERS measurements. The wrinkled nanoporous structure was maintained after multiple mild plasma treatments for reuse. The simplicity of plasma-based fabrication and high sensitivity of w-npAgFs are promising features for the green production of low-cost and reusable 3D SERS substrates.

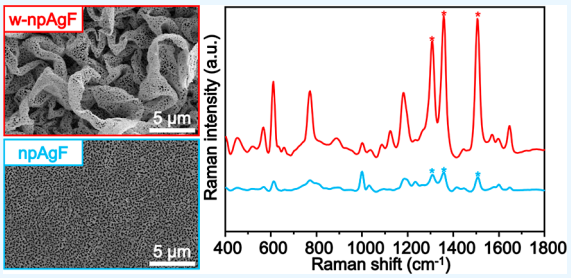

1. INTRODUCTION

Surface-enhanced Raman spectroscopy (SERS) is a promising chemical sensing technique because of the large amplification of the Raman signal of target molecules providing vibrational information.[1−3] Strong light amplification on the surface of noble-metal nanostructures by the localized surface plasmon resonance (LSPR) effect can considerably enhance the Raman signal from nearby molecules.[4,5]

Because light enhancement can be maximized in the small gap between nanostructures, called hot spots, various plasmonic nanostructures, from colloidal nanoparticle aggregates to lithographically patterned substrates, have been used for SERS.[3,6−10] Among them, a nanoporous structure, comprising numerous interconnected nanosized plasmonic metal ligaments, is promising owing to its large surface area for adsorbing probe molecules as well as abundant hot spots inside its nanopores.[11−19] Furthermore, it exhibits superior robustness and reproducibility than a colloidal nanoparticle aggregate randomly induced in the solution phase.

Among the two most representative noble metals, gold and silver, which exhibit LSPR in the visible-to-near-infrared (vis-NIR) wavelength range, silver is more cost-effective and exhibits LSPR stronger than does gold. However, its use is often limited owing to its vulnerability to oxidation, because oxidized silver does not exhibit as strong LSPR as pristine silver nanostructures.[20,21] Therefore, gold is preferred for practical applications.

Nanoporous noble-metal films have mostly been fabricated using the dealloying method, in which the less noble metal is selectively removed from a metal alloy using a strong acid to leave a bicontinuous nanoporous structure.[16,17] For example, a nanoporous gold film (npAuF) can be fabricated by dealloying a Au−Ag alloy,[13,22] while a nanoporous silver film (npAgF) can be fabricated by dealloying a Ag−Al alloy.[23,24] However, dealloying requires the prefabrication of alloys including sacrificial metals in an appropriate ratio and uses environmentally unfriendly corrosive chemicals for etching.

Alternatively, a template-mediated method using sacrificial templates has also been developed to fabricate nanoporous noble-metal structures.[25,26] Although corrosive chemicals are not required for this method, additional processes are required to prepare a nanoporous template and to remove it after the production of a nanoporous metal film.

Received: September 18, 2023
Revised: November 9, 2023
Accepted: November 22, 2023
Published: December 4, 2023

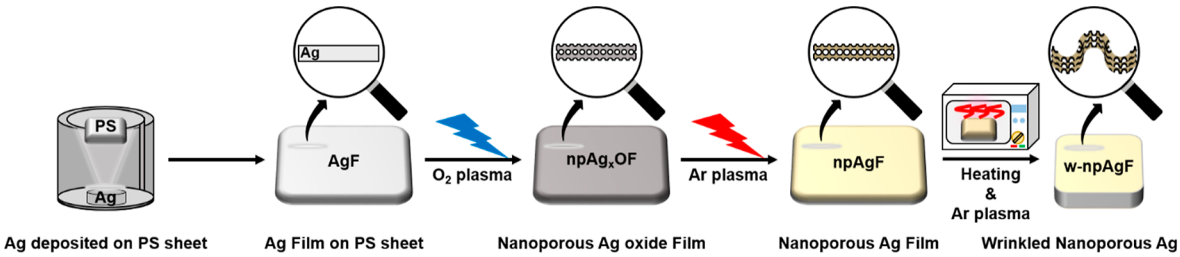

Figure 1. Schematic of the fabrication procedure for the w-npAgF. Detailed fabrication conditions are described in the Experimental Section.

Recently, an interesting method for preparing an npAgF from a planar Ag film using oxygen plasma was reported by Ma et al.[27] Oxygen plasma has been widely used for removing organic materials or polymer templates from various substrates such as glass, silicon, and gold,[28−30] whereas it has seldom been used for silver structures because silver can be easily oxidized resulting in damage of its structure. However, Ma et al. deliberately induced the strong oxidation of silver using oxygen plasma to produce the npAgF. Internal stress induced by the oxide layer growth on the surface of silver can cause cracking and roughness of the surface, and the repetition of this process finally results in a nanoporous silver oxide film ($npAg_xOF$).[27,31] Furthermore, it was reported that post-treatment with sodium citrate or argon plasma could reduce the $npAg_xOF$ structure to the pristine npAgF with high SERS activity.[27,31,32]

The plasma-based fabrication of an npAgF is facile and produces a uniform nanoporous structure on a large scale. Unlike the dealloying method, it does not require an annealing process at high temperatures to produce an alloy film or a harsh etching process using corrosive chemicals. Thus, it can be directly applied to various substrates, such as filter paper, polystyrene (PS) film, and aluminum foil.[27] This can allow post-treatment of the substrate to produce more sophisticated npAgF structures by using the unique characteristics of the substrate, such as flexibility and contractibility.

Herein, we report a facile fabrication method for wrinkled npAgFs (w-npAgFs) on a PS substrate for SERS applications. After an npAgF was fabricated by applying consecutive O_2 and Ar plasmas to the thermally deposited Ag film on the prestrained PS substrate, quasi-periodic 3D wrinkles of the npAgF were formed by the thermal contraction of the prestrained PS substrate with the npAgF.

Studies have reported that the buckling of thin metal films by the thermal contraction of an underlying substrate can produce wrinkled films.[33,34] The close approach of plasmonic nanoparticles or formation of nanogaps between nanopetals induced by wrinkling considerably enhances the local electromagnetic field, which can be used for SERS or metal-enhanced fluorescence.[35−37] Previously, a wrinkled npAuF (w-npAuF) was fabricated for SERS applications by the transfer of a dealloyed free-standing npAuF onto the prestrained PS substrate and subsequent thermal contraction.[38,39] However, unlike those in the dealloying-based fabrication of a w-npAuF, all the steps in our plasma-based fabrication of w-npAgFs are basically dry processes that do not require a wet-etching process using corrosive chemicals or the transfer of film to different substrates. Therefore, it is environmentally friendly and simple.

The 3D wrinkles of the npAgF maintained its nanoporous structure and showed approximately 8 times higher SERS enhancement than did the flat npAgF. We also demonstrated that the w-npAgF can be reused for multiple SERS measurements of different molecules using mild O_2 and Ar plasma treatments after each use. The O_2 plasma could effectively remove adsorbed organic molecules and the Ar plasma could restore the pristine npAgF for subsequent SERS measurements. Scanning electron microscopy (SEM) images confirmed that the wrinkled nanoporous structure was maintained for reuse after multiple plasma treatments.

2. EXPERIMENTAL SECTION

2.1. Materials. A silver wire (φ1 × 10 mm long) for the thermal deposition of the silver film was purchased from Woo Jin Chemical (Seoul, Korea). The thermally contractible, prestrained PS substrate (KSF50, Grafix Shrink Film) was purchased from Grafix (Ohio, USA). Rhodamine 6G (R6G), crystal violet (CV), methylene blue (MB), and 4-aminothiophenol (4-ATP) were purchased from Sigma-Aldrich (Darmstadt, Germany). Deionized (DI) water (18.2 MΩ·cm) was prepared by using a Milli-Q system (Millipore).

2.2. Fabrication of the w-npAgF. The properly cut prestrained PS substrates were cleaned in isopropanol for 1 min with sonication, rinsed with DI water, and dried by N_2 blowing. Before loading the PS substrates in the thermal evaporator for the deposition of the Ag film, the surface of the PS substrates was activated by O_2 plasma for 1 min for better adhesion of the Ag film. Then, a 100 nm thick Ag film was deposited on the PS substrates at a rate of 1 Å/s by thermal vacuum evaporation under a pressure of 6.0×10^{-6} Torr. The Ag-film-deposited PS substrates were cut into 1 × 1 cm^2 pieces for plasma treatment to produce npAgFs. When the pressure of the plasma chamber (PDC-32G-2, Harrick plasma) was approximately 190 mTorr, the reaction gas was injected and radio frequency power was applied. The Ag-film-deposited PS substrates were first treated with O_2 plasma (8 sccm, 11 W) for 6 min and then with Ar plasma (12 sccm, 11 W) for 6 min to produce npAgFs. To fabricate the w-npAgF, the fabricated npAgF was heated at 140 °C for 1 min in a minielectric oven (Tefal) after the oven was preheated. After heating, the w-npAgF was treated again with mild Ar plasma (12 sccm, 7 W, 4 min) to remove possible silver oxidation before use for SERS measurements.

2.3. Characterizations and SERS Measurements. The morphologies of the npAgF and w-npAgF were investigated using ultrahigh-resolution field-emission SEM (UHR FE-SEM, Verios 5 UC, ThermoFisher, USA). The X-ray diffraction (XRD) patterns were measured using a multipurpose X-ray diffractometer (SmartLab, Rigaku, Japan, Cu Kα) and analyzed using analytical software (SmartLab Studio II, PDF-2). For the SERS measurements, dye solutions of R6G and CV in ethanol and MB in water were prepared. The npAgF and w-npAgF substrates were dipped in 5 mL of dye solutions at specific

https://doi.org/10.1021/acsomega.3c07167
ACS Omega 2023, 8, 47146−47152

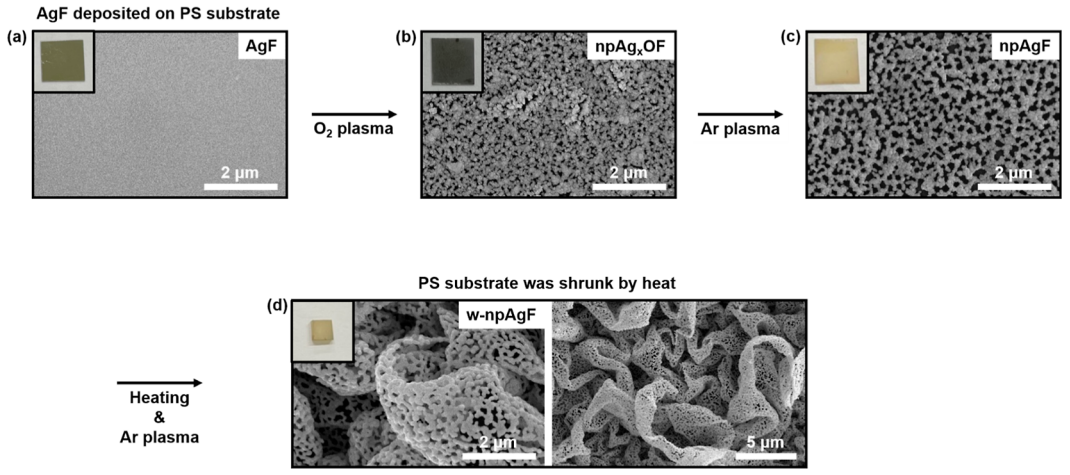

Figure 2. SEM images of the (a) 100 nm-thick planar AgF deposited on the PS substrate, (b) $npAg_xOF$ after O_2 plasma treatment, (c) npAgF after Ar plasma treatment, and (d) w-npAgF structures at two different scales after thermal contraction of the PS substrate. The insets show photos of each substrate.

concentrations overnight and then rinsed with each solvent. To calculate the limit of detection (LOD) for 4-ATP, the increasing concentration of 4-ATP in ethanol solution was prepared, and 10 μL of each solution was dropped on the w-npAgF. After drying, the Raman spectra of the substrates were measured at room temperature using a custom-built Raman system. The excitation light was a 785 nm continuous wave laser with a power of 8.5 mW for the sample. The Raman signal was detected using an NA 0.22 Raman probe (RIP-RPB-785, Ocean Optics) for an acquisition time of 0.1 s with 100 accumulations.

3. RESULTS AND DISCUSSION

Figure 1 shows a schematic of the procedure for the fabrication of the w-npAgF, and Figure 2 shows the corresponding SEM images. First, a 100 nm Ag film was deposited onto the prestrained PS substrate using a thermal evaporator (Figure 2a). Before the deposition of the Ag film, the surface of the PS substrate was treated with O_2 plasma for 1 min for better adhesion of the Ag film. Generally, a thin adhesion layer of Cr or Au is necessary for adequate adhesion of a Ag film on a glass or Si substrate.[31] However, for a PS substrate, surface activation by O_2 plasma, instead of an additional Cr adhesion layer, was effective for adequate adhesion of the Ag film on the substrate.[40]

The Ag film deposited on the PS substrate was treated with O_2 plasma (8 sccm, 11 W) for 6 min to induce strong oxidation of the silver surface. The internal stress accumulated during the rapid growth of the oxide layer caused repetitive cracking and finally resulted in a porous structure with pore sizes on the order of 100 nm, as confirmed by SEM (Figure 2b).[31] The XRD patterns show peaks of silver oxides (AgO/Ag_2O) without distinct Ag peaks (Figure 3). The peaks at 2θ = 32.2 and 37.2° of the $npAg_xOF$ correspond to the (111) and (200) Bragg peaks of AgO (ICDD 01-076-1489) or Ag_2O (ICDD 01-078-5868), respectively, with a cubic structure. This demonstrates almost complete oxidation of the Ag film owing to the small thickness (100 nm) of the AgF. This structure is designated as $npAg_xOF$.[27]

The $npAg_xOF$ was further treated with Ar plasma (12 sccm, 11 W) for 6 min to reduce Ag_xO to pristine Ag (npAgF). The XRD pattern of the npAgF shows only Ag peaks. The peaks at

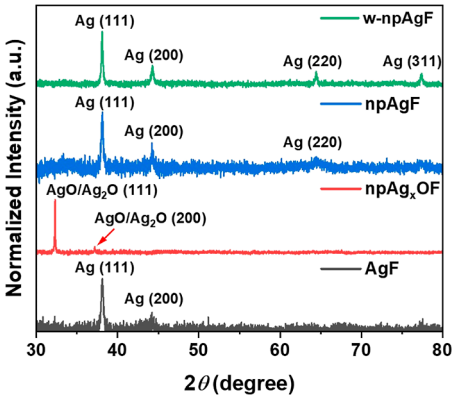

Figure 3. XRD patterns of AgF, $npAg_xOF$, npAgF, and w-npAgF.

2θ = 38.1 and 44.2° correspond to the (111) and (200) Bragg peaks of Ag, respectively, with a cubic structure (ICDD 01-073-6859). This demonstrates the complete reduction of Ag_xO to pristine Ag. The npAgF exhibits slightly larger pores than does the $npAg_xOF$ (Figure 2c). This is attributed to volume contraction due to the removal of oxygen during the reduction of Ag_xO to Ag. The average pore diameter was evaluated to be 156 nm for 353 pores by ImageJ analysis (Figure S1).

To prepare the w-npAgF, the fabricated npAgF on a prestrained PS substrate was heated at 140 °C for 1 min in an oven under atmospheric pressure. By heating above the glass transition temperature of PS (~95 °C), the prestrained PS substrate contracted to 16% of the original area ($\Delta L/L_{orig.}$ = 0.6, $\Delta A/A_{orig.}$ = 0.84). This induced wrinkles in the npAgF on the PS substrate (Figure 2d).[38] The w-npAgF maintained the original nanoporous structure of the nonwrinkled npAgF but was more three-dimensional due to the increased height of the wrinkles. This 3D characteristic of wrinkles is advantageous for the adsorption of molecules because it increases the effective surface area per projection area. Moreover, the w-npAgF has a hierarchical structure consisting of both micrometer-sized wrinkles and 100 nanometer-sized nanopores, which can further facilitate the transport and adsorption of molecules on the surface of the w-npAgF. To exclude the effect of possible oxidation during heating in the oven, the w-npAgF was treated again by mild Ar plasma (12 sccm, 7 W, 4 min) after heating

https://doi.org/10.1021/acsomega.3c07167
ACS Omega 2023, 8, 47146−47152

before use for SERS measurements. This is confirmed by the XRD pattern, in which only pristine Ag peaks, and no Ag oxide peaks, are identified (Figure 3). The plasma treatment and heating did not induce a change in the crystallinity of the film, as demonstrated by the similar fwhm of Ag(111) peaks in all three structures of the w-npAgF, npAgF, and AgF (Figure S2).

To estimate the contribution of wrinkles to SERS enhancement, the Raman intensity from R6G adsorbed on the w-npAgF was compared with those on the npAgF and AgF (Figure 4). For sufficient adsorption of R6G on the Ag surface,

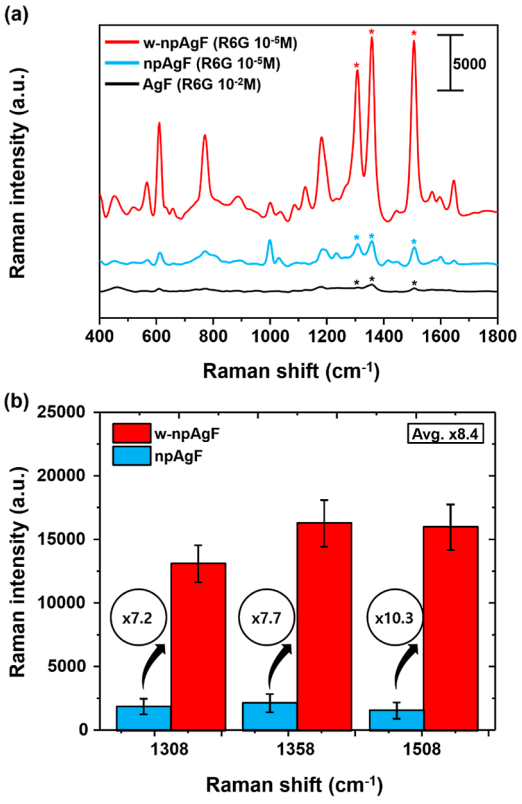

Figure 4. (a) Raman spectra of R6G adsorbed on the different substrates at concentrations of 10^{-2} M for the AgF and 10^{-5} M for the npAgF and w-npAgF. The spectra were acquired with 785 nm excitation. The three representative peaks of R6G at 1308, 1358, and 1508 cm^{-1} are marked with asterisks. (b) Comparison of the Raman intensities from the npAgF and w-npAgF at three representative peaks of R6G. Error bars represent the standard deviation of Raman intensities acquired from 20 random regions of three similarly fabricated substrates for both the npAgF and w-npAgF.

the substrates were immersed overnight in a solution of R6G in ethanol and then rinsed with ethanol. An excitation laser of 785 nm wavelength (8.5 mW power at the sample) was used for the nonresonant Raman scattering measurements to minimize fluorescence and photobleaching of R6G, and the Raman signal was detected using a Raman probe for an acquisition time of 0.1 s with 100 accumulations. The baseline of the Raman spectra was corrected by subtracting the fluorescence background.[41]

While the planar AgF shows weak Raman spectra even at the R6G concentration of 10 mM, the npAgF and w-npAgF show strong Raman peaks compared to the planar AgF at 1000 times lower concentrations. The Raman peaks of the w-npAgF are much stronger than those of the npAgF. The contribution of wrinkles to the SERS enhancement was evaluated by comparing the Raman intensities of three representative peaks of R6G at 1308, 1358, and 1508 cm^{-1}.[15,42,43] To compare the average Raman intensity, we measured and averaged the Raman intensities of 20 random regions for each of three similarly fabricated substrates, for both the npAgF and w-npAgF. Since the Raman probe of NA 0.22 (RIP-RPB-785, Ocean Optics), not the micro-Raman setup with high NA objective, was used for SERS measurements in our experiment, signal fluctuation due to the substrate inhomogeneity on the micrometer-scale wrinkles was not significant. (Standard deviation was approximately 11% for three representative peaks of R6G from the w-npAgF, Figure 4b).

The w-npAgF shows an approximately 8.4 times higher SERS intensity than does the npAgF on average for three peaks (7.2 times for the 1308 cm^{-1} peak, 7.7 times for the 1358 cm^{-1} peak, and 10.3 times for the 1508 cm^{-1} peak). The analytical enhancement factors (AEFs) of the npAgF and w-npAgF were estimated to be $\sim 5.8 \times 10^4$ and $\sim 4.5 \times 10^5$, respectively, for the 1358 cm^{-1} peak of R6G (Figure S3, Supporting Information). This increment should be mostly caused by the increased number of adsorbed molecules per projection area due to the 3D wrinkle formation by the geometric contraction of the area (1/0.16 = 6.25 times). In addition, more vertically standing films in the wrinkled structure can be advantageous for coupling with the laterally oscillating electromagnetic field of vertically incident laser light.[38] Moreover, possible cracking of the surface or close approach of adjacent wrinkles can generate new hot spots and additionally contribute to the SERS enhancement, although it is not the dominant factor.

Notably, the wrinkle-induced increment in our npAgF is smaller than the previously reported value in the npAuF fabricated using the dealloying method, probably due to the difference in pore and ligament sizes.[38] The dealloying method can produce much smaller pores and ligaments (several tens of nanometers) than the plasma-induced method, and these small ligaments can induce many sharp-cut crack edges due to the fractured ligaments during formation of wrinkles. However, it was hard to obtain the ligaments of several tens of nanometers of thickness in the plasma-treated npAgF and these thick ligaments were more plastically deformed rather than forming sharp cracks during wrinkling. However, considering the simplicity and eco-friendliness of the plasma-based fabrication of the npAgF, it is still meaningful that an additional 8.4-fold increase in SERS intensity can be attained by simple wrinkle formation.

The fabricated w-npAgF was also applied for the SERS measurement of different organic molecules, 4-ATP. Since the 4-ATP has a thiol group, it can strongly bind to the surface of the npAgF. The SERS intensity at 1076 cm^{-1} from different concentrations of 4-ATP on the w-npAgF showed a linear relationship (R^2 of 0.996) in the log–log scale for the range of 10^{-3}–10^{-7} M (Figure 5a,b). The LOD was calculated to be 9.7×10^{-8} M from 3.3 times the standard deviation of the blank samples.

Another advantage of plasma treatment is the reusability of the w-npAgF substrate in SERS applications. O_2 plasma can effectively remove organic molecules adsorbed onto substrates. Thus, the O_2 plasma treatment has been used for cleaning various substrates; however, it has seldom been used for Ag substrates because of the undesirable oxidation of Ag. By contrast, although Ar plasma does not cause oxidation, it is less effective than O_2 plasma in removing organic molecules.[44]

https://doi.org/10.1021/acsomega.3c07167
ACS Omega 2023, 8, 47146−47152

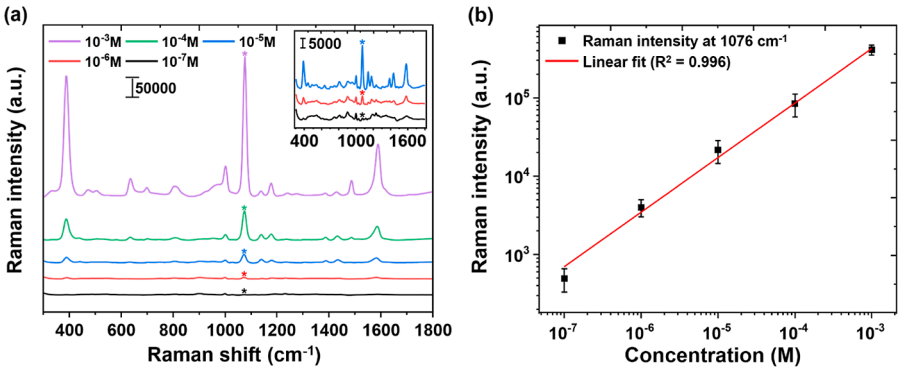

Figure 5. (a) Raman spectra for different concentrations (from 10^{-3} to 10^{-7} M) of 4-ATP adsorbed on the w-npAgF. The magnified spectra for low concentrations (from 10^{-5} to 10^{-7} M) are shown in the inset for clarity. (b) Raman intensity at 1076 cm^{-1} (the representative peak of 4-ATP) was plotted for different concentrations of 4-ATP. Error bars represent the standard deviation of Raman intensities acquired from 15 random regions of the w-npAgF.

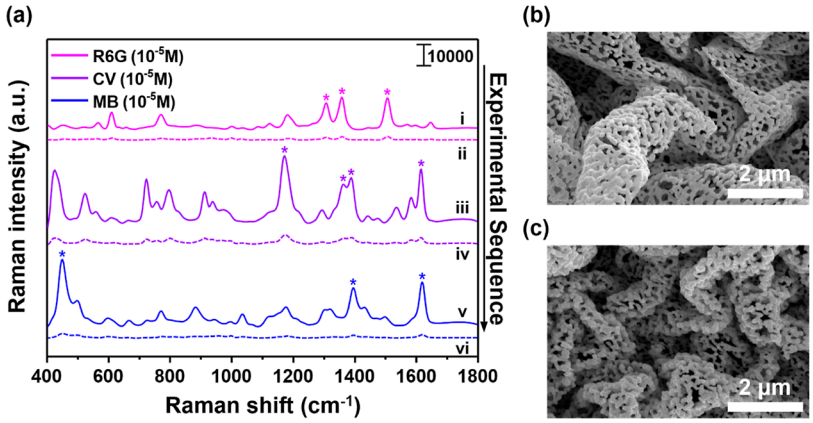

Figure 6. (a) SERS spectra from sequential measurements in the order of (i) R6G-adsorbed, (ii) plasma-cleaned, (iii) CV-adsorbed, (iv) plasma-cleaned, (v) MB-adsorbed, and (vi) plasma-cleaned same w-npAgF substrates. After plasma cleaning, the SERS peaks from previous dyes almost disappeared, enabling new SERS measurements using the same substrate for subsequent dyes. Comparison of SEM images of the (b) freshly fabricated w-npAgF before any SERS measurement and (c) w-npAgF after three repeated SERS measurements and plasma-cleaning processes.

Consecutive O_2 and Ar plasma treatments can resolve both effectiveness and oxidation issues by first effectively removing the organic molecules using O_2 plasma and then reducing the Ag oxides to pristine Ag using Ar plasma.

We demonstrated that short O_2 and Ar plasma treatments at a low plasma power of 7 W could effectively remove the organic molecules adsorbed on the w-npAgF without affecting its original wrinkled nanoporous structure. The cleaned w-npAgF substrates could be reused for SERS measurements of different dyes without interference from their spectra. Figure 6 shows the SERS spectra obtained from three consecutive SERS measurements of different dyes: R6G, CV, and MB using the same w-npAgF substrate.[43,45] After the SERS measurement for each dye, the w-npAgF substrate was cleaned using O_2 plasma (8 sccm) and then Ar plasma (12 sccm) for 4 min each, at a plasma power of 7 W before applying for the next SERS measurement of new dyes. Because the SERS peaks from the previous dyes mostly disappeared after each plasma treatment, the same w-npAgF substrate could be reused for subsequent SERS measurements in which the representative SERS peaks of the corresponding dye could be distinctly identified without significant interference from those of previous dyes. We also checked the recovery of SERS intensity for the same dye, and it was found that approximately half of the initial SERS intensity can be recovered even after 5 cycles of cleaning and measurements (Figure S4).

We confirmed that multiple O_2 and Ar plasma treatments did not affect the original structure of w-npAgFs. The SEM image of the w-npAgF after three rounds of O_2 and Ar plasma treatments for cleaning is similar to that of the original w-npAgF (Figure 6b,c). By contrast, multiple O_2 and Ar plasma treatments at a higher power (11 W) induced the fusion of Ag ligaments, resulting in the disappearance of nanopores even after treatment for 30 s (Figure S5). Therefore, under our experimental conditions, mild O_2 and Ar plasma treatments at a low power (7 W) were necessary to maintain the original wrinkled nanoporous structure of a w-npAgF for multiple reuses.

Previously, research revealed that an Ar plasma of 16.7 sccm at a plasma power of 50 W for 5 min could completely remove the 10^{-6} M rhodamine B adsorbed on the npAgF, although the SEM images of the npAgF before and after the plasma treatment were not compared.[32] However, Ar plasma treatment alone, using our plasma instrument (maximum power of 18 W), could not completely remove dyes adsorbed on the w-npAgF, probably because Ar plasma is less effective in removing organic molecules than O_2 plasma at the same power.

https://doi.org/10.1021/acsomega.3c07167
ACS Omega 2023, 8, 47146−47152

4. CONCLUSIONS

We successfully fabricated a w-npAgF with both micrometer-scale 3D wrinkles and 100 nanometer-scale nanopores by applying successive O_2 and Ar plasma treatments to a planar silver film deposited on a thermally contractible, prestrained PS substrate. Owing to its 3D hierarchical structure, the w-npAgF had a large surface area for molecular adsorption per unit of projection area. Moreover, the bending of the nanoporous film or the close approach of adjacent wrinkles could generate additional hot spots. For these reasons, the w-npAgF showed an 8.4 times higher sensitivity than did the nonwrinkled npAgF for the SERS measurement of R6G. The AEF of the w-npAgF was estimated to be 4.5×10^5 for a 1358 cm^{-1} peak of R6G with 785 nm laser excitation. The LOD for 4-ATP using the w-npAgF was calculated to be 9.7×10^{-8} M. The w-npAgF could also be reused for multiple SERS measurements of different dyes after mild O_2 and Ar plasma cleaning, which did not change the original wrinkled nanoporous structure, as confirmed by SEM. As these fabrication and cleaning methods for w-npAgFs do not require any wet-etching process using corrosive or toxic chemicals, they are environmentally friendly and simple. Therefore, the plasma-based fabrication of w-npAgFs is a promising Ag-based 3D SERS platform for the green production of low-cost, sensitive, and reusable SERS substrates.

ASSOCIATED CONTENT

Supporting Information

The Supporting Information is available free of charge at https://pubs.acs.org/doi/10.1021/acsomega.3c07167.

Image analysis for pore size distribution of the npAgF, enlarged XRD graphs, Raman spectra of normal substrates, enhancement factor calculation, SERS intensity from R6G for multiple uses of the w-npAgF, and FE-SEM images of the w-npAgF before and after plasma-cleaning processes (PDF)

AUTHOR INFORMATION

Corresponding Authors

Myoung-Kyu Oh − *Advanced Photonics Research Institute (APRI), Gwangju Institute of Science and Technology, Gwangju 61005, Republic of Korea*; Email: omkyu@gist.ac.kr

Joon Heon Kim − *Advanced Photonics Research Institute (APRI), Gwangju Institute of Science and Technology, Gwangju 61005, Republic of Korea*; orcid.org/0000-0002-9803-2830; Email: joonhkim@gist.ac.kr

Authors

Jin-Hyun Ham − *Advanced Photonics Research Institute (APRI), Gwangju Institute of Science and Technology, Gwangju 61005, Republic of Korea*

Jung Su Park − *Advanced Photonics Research Institute (APRI), Gwangju Institute of Science and Technology, Gwangju 61005, Republic of Korea*

Complete contact information is available at: https://pubs.acs.org/10.1021/acsomega.3c07167

Notes

The authors declare no competing financial interest.

ACKNOWLEDGMENTS

This research was supported by the National Research Foundation of Korea (NRF) grant funded by the MSIT of the Korean government (NRF-2018R1A2B6007730, NRF-2021R1A2C1008787) and by the GIST Research Institute (GRI) grant funded by the GIST in 2023.

REFERENCES

(1) Langer, J.; Jimenez de Aberasturi, D.; Aizpurua, J.; Alvarez-Puebla, R. A.; Auguié, B.; Baumberg, J. J.; Bazan, G. C.; Bell, S. E. J.; Boisen, A.; Brolo, A. G.; Choo, J.; Cialla-May, D.; Deckert, V.; Fabris, L.; Faulds, K.; García de Abajo, F. J.; Goodacre, R.; Graham, D.; Haes, A. J.; Haynes, C. L.; Huck, C.; Itoh, T.; Käll, M.; Kneipp, J.; Kotov, N. A.; Kuang, H.; le Ru, E. C.; Lee, H. K.; Li, J. F.; Ling, X. Y.; Maier, S. A.; Mayerhöfer, T.; Moskovits, M.; Murakoshi, K.; Nam, J. M.; Nie, S.; Ozaki, Y.; Pastoriza-Santos, I.; Perez-Juste, J.; Popp, J.; Pucci, A.; Reich, S.; Ren, B.; Schatz, G. C.; Shegai, T.; Schlücker, S.; Tay, L. L.; Thomas, K. G.; Tian, Z. Q.; van Duyne, R. P.; Vo-Dinh, T.; Wang, Y.; Willets, K. A.; Xu, C.; Xu, H.; Xu, Y.; Yamamoto, Y. S.; Zhao, B.; Liz-Marzán, L. M. Present and Future of Surface-Enhanced Raman Scattering. *ACS Nano* **2020**, *14*, 28−117.

(2) Pérez-Jiménez, A. I.; Lyu, D.; Lu, Z.; Liu, G.; Ren, B. Surface-enhanced Raman spectroscopy: benefits, trade-offs and future developments. *Chem. Sci.* **2020**, *11* (18), 4563−4577.

(3) Ding, S.-Y.; Yi, J.; Li, J.-F.; Ren, B.; Wu, D.-Y.; Panneerselvam, R.; Tian, Z.-Q. Nanostructure-based plasmon-enhanced Raman spectroscopy for surface analysis of materials. *Nat. Rev. Mater.* **2016**, *1*, 16021−16036.

(4) Lim, D.-K.; Jeon, K.-S.; Hwang, J.-H.; Kim, H.; Kwon, S.; Suh, Y. D.; Nam, J.-M. Highly uniform and reproducible surface-enhanced Raman scattering from DNA-tailorable nanoparticles with 1-nm interior gap. *Nat. Nanotechnol.* **2011**, *6*, 452−460.

(5) Stiles, P. L.; Dieringer, J. A.; Shah, N. C.; Van Duyne, R. P. Surface-enhanced Raman spectroscopy. *Annu. Rev. Anal. Chem.* **2008**, *1*, 601−626.

(6) De Silva Indrasekara, A. S. Design criteria to fabricate plasmonic gold nanomaterials for surface-enhanced Raman scattering (SERS)-based biosensing. *J. Appl. Phys.* **2021**, *129*, 231102.

(7) Huang, Y.; Chen, Y.; Wang, L.-L.; Ringe, E. Small morphology variations effects on plasmonic nanoparticle dimer hotspots. *J. Mater. Chem. C* **2018**, *6*, 9607−9614.

(8) Yang, M.; Alvarez-Puebla, R.; Kim, H.-S.; Aldeanueva-Potel, P.; Liz-Marzán, L. M.; Kotov, N. A. SERS-active gold lace nanoshells with built-in hotspots. *Nano Lett.* **2010**, *10*, 4013−4019.

(9) Im, H.; Bantz, K. C.; Lindquist, N. C.; Haynes, C. L.; Oh, S.-H. Vertically oriented sub-10-nm plasmonic nanogap arrays. *Nano Lett.* **2010**, *10* (6), 2231−2236.

(10) Chen, A.; DePrince, A. E.; Demortière, A.; Joshi-Imre, A.; Shevchenko, E. V.; Gray, S. K.; Welp, U.; Vlasko-Vlasov, V. K. Self-assembled large Au nanoparticle arrays with regular hot spots for SERS. *Small* **2011**, *7*, 2365−2371.

(11) Koya, A. N.; Zhu, X.; Ohannesian, N.; Yanik, A. A.; Alabastri, A.; Proietti Zaccaria, R.; Krahne, R.; Shih, W.-C.; Garoli, D. Nanoporous Metals: From Plasmonic Properties to Applications inEnhanced Spectroscopy and Photocatalysis. *ACS Nano* **2021**, *15* (4), 6038−6060.

(12) Kucheyev, S. O.; Hayes, J. R.; Biener, J.; Huser, T.; Talley, C. E.; Hamza, A. V. Surface-enhanced Raman scattering on nanoporous Au. *Appl. Phys. Lett.* **2006**, *89* (5), 053102.

(13) Qian, L. H.; Yan, X. Q.; Fujita, T.; Inoue, A.; Chen, M. W. Surface enhanced Raman scattering of nanoporous gold: Smaller pore sizes stronger enhancements. *Appl. Phys. Lett.* **2007**, *90* (15), 153120.

(14) Zhao, F.; Zeng, J.; Parvez Arnob, M. M.; Sun, P.; Qi, J.; Motwani, P.; Gheewala, M.; Li, C.-H.; Paterson, A.; Strych, U.; Raja, B.; Willson, R. C.; Wolfe, J. C.; Lee, T. R.; Shih, W.-C. Monolithic NPG nanoparticles with large surface area, tunable plasmonics, and high-density internal hot-spots. *Nanoscale* **2014**, *6* (14), 8199−8207.

(15) Jeong, S.; Kim, M.-W.; Jo, Y.-R.; Kim, N.-Y.; Kang, D.; Lee, S. Y.; Yim, S.-Y.; Kim, B.-J.; Kim, J. H. Hollow porous gold nanoshells with controlled nanojunctions for highly tunable plasmon resonances and intense field enhancements for surface-enhanced Raman Scattering. *ACS Appl. Mater. Interfaces* **2019**, *11*, 44458−44465.
(16) Zhang, R.; Olin, H. Porous gold films - a short review on recent progress. *Materials* **2014**, *7*, 3834−3854.
(17) Ding, Y.; Chen, M. Nanoporous metals for catalytic and optical applications. *MRS Bull.* **2009**, *34* (8), 569−576.
(18) Chen, L.-Y.; Yu, J.-S.; Fujita, T.; Chen, M.-W. Nanoporous copper with tunable nanoporosity for SERS applications. *Adv. Funct. Mater.* **2009**, *19*, 1221−1226.
(19) Li, M.; Zhao, F.; Zeng, J.; Qi, J.; Lu, J.; Shih, W. C. Microfluidic surface-enhanced Raman scattering sensor with monolithically integrated nanoporous gold disk arrays for rapid and label-free biomolecular detection. *J. Biomed. Opt.* **2014**, *19* (11), 111611.
(20) Kim, N.-Y.; Leem, Y.-C.; Hong, S.-H.; Park, J.-H.; Yim, S.-Y. Ultrasensitive and stable plasmonic surface-enhanced Raman scattering substrates covered with atomically thin monolayers: Effect of the insulating property. *ACS Appl. Mater. Interfaces* **2019**, *11*, 6363−6373.
(21) Han, Y.; Lupitskyy, R.; Chou, T.-M.; Stafford, C. M.; Du, H.; Sukhishvili, S. Effect of oxidation on surface-enhanced Raman scattering activity of silver nanoparticles: a quantitative correlation. *Anal. Chem.* **2011**, *83*, 5873−5880.
(22) Ding, Y.; Kim, Y.-J.; Erlebacher, J. Nanoporous gold leaf: "Ancient technology"/advanced material. *Adv. Mater.* **2004**, *16* (21), 1897−1900.
(23) Qiu, H.; Zhang, Z.; Huang, X.; Qu, Y. Dealloying Ag-Al alloy to prepare nanoporous silver as a substrate for surface-enhanced raman scattering: effects of structural evolution and surface modification. *ChemPhysChem* **2011**, *12* (11), 2118−2123.
(24) Wang, X.; Qi, Z.; Zhao, C.; Wang, W.; Zhang, Z. Influence of alloy composition and dealloying solution on the formation and microstructure of monolithic nanoporous silver through chemical dealloying of Al-Ag alloys. *J. Phys. Chem. C* **2009**, *113*, 13139−13150.
(25) Kwon, H.; Barad, H. N.; Silva Olaya, A. R.; Alarcón-Correa, M.; Hahn, K.; Richter, G.; Wittstock, G.; Fischer, P. Dry Synthesis of Pure and Ultrathin Nanoporous Metallic Films. *ACS Appl. Mater. Interfaces* **2023**, *15* (4), 5620−5627.
(26) Zhang, L.; Jaroniec, M. Strategies for development of nanoporous materials with 2D building units. *Chem. Soc. Rev.* **2020**, *49*, 6039−6055.
(27) Ma, C.; Trujillo, M. J.; Camden, J. P. Nanoporous silver film fabricated by oxygen plasma: A Facile Approach for SERS Substrates. *ACS Appl. Mater. Interfaces* **2016**, *8* (36), 23978−23984.
(28) Jung, M.-H.; Choi, H.-S. Photoresist etching using Ar/O2 and He/O2 atmospheric pressure plasma. *Thin Solid Films* **2006**, *515* (4), 2295−2302.
(29) Lotito, V.; Zambelli, T. Manipulating the morphology of colloidal particles via ion beam irradiation: A route to anisotropic shaping. *Adv. Colloid Interface Sci.* **2022**, *304*, 102642.
(30) Lee, D. H.; Park, J. S.; Hwang, J. H.; Kang, D.; Yim, S.-Y.; Kim, J. H. Fabrication of hollow nanoporous gold nanoshells with high structural tunability based on the plasma etching of polymer colloid templates. *J. Mater. Chem. C* **2018**, *6*, 6194−6199.
(31) Capaccio, A.; Sasso, A.; Rusciano, G. A simple and reliable approach for the fabrication of nanoporous silver patterns for surface-enhanced Raman spectroscopy applications. *Sci. Rep.* **2021**, *11* (1), 22295.
(32) Okeil, S.; Schneider, J. J. Controlling surface morphology and sensitivity of granular and porous silver films for surface-enhanced Raman scattering, SERS. *Beilstein J. Nanotechnol.* **2018**, *9* (1), 2813−2831.
(33) Mei, Y.; Kiravittaya, S.; Harazim, S.; Schmidt, O. G. Principles and applications of micro and nanoscale wrinkles. *Mater. Sci. Eng. R Rep.* **2010**, *70*, 209−224.
(34) Fu, C.-C.; Grimes, A.; Long, M.; Ferri, C. G. L.; Rich, B. D.; Ghosh, S.; Ghosh, S.; Lee, L. P.; Gopinathan, A.; Khine, M. Tunable nanowrinkles on shape memory polymer sheets. *Adv. Mater.* **2009**, *21*, 4472−4476.
(35) Gabardo, C. M.; Yang, J.; Smith, N. J.; Adams-McGavin, R. C.; Soleymani, L. Programmable wrinkling of self-assembled nanoparticle films on shape memory polymers. *ACS Nano* **2016**, *10* (9), 8829−8836.
(36) Mengesha, Z. T.; Yang, J. Silver nanoparticle-decorated shape-memory polystyrene sheets as highly sensitive surface-enhanced Raman scattering substrates with a thermally inducible hot spot effect. *Anal. Chem.* **2016**, *88*, 10908−10915.
(37) Fu, C.-C.; Ossato, G.; Long, M.; Digman, M. A.; Gopinathan, A.; Lee, L. P.; Gratton, E.; Khine, M. Bimetallic nanopetals for thousand-fold fluorescence enhancements. *Appl. Phys. Lett.* **2010**, *97*, 203101.
(38) Zhang, L.; Lang, X.; Hirata, A.; Chen, M. Wrinkled nanoporous gold films with ultrahigh surface-enhanced Raman scattering enhancement. *ACS Nano* **2011**, *5* (6), 4407−4413.
(39) Liu, H.; Zhang, L.; Lang, X.; Yamaguchi, Y.; Iwasaki, H.; Inouye, Y.; Xue, Q.; Chen, M. Single molecule detection from a large-scale SERS-active Au79Ag21 substrate. *Sci. Rep.* **2011**, *1*, 112.
(40) Paproth, A.; Wolter, K.-J.; Deltschew, R. Adhesion of metal/polymer bonds using PBT, PC, PS and copper. *Proceedings of 56th Electronic Components and Technology Conference (IEEE)*: San Diego, CA, USA, 2006; pp 959−963.
(41) Zhao, J.; Lui, H.; McLean, D. I.; Zeng, H. Automated autofluorescence background subtraction algorithm for biomedical Raman spectroscopy. *Appl. Spectrosc.* **2007**, *61*, 1225−1232.
(42) Chan, S.; Kwon, S.; Koo, T.-W.; Lee, L. P.; Berlin, A. A. Surface-enhanced Raman scattering of small molecules from silver-coated silicon nanopores. *Adv. Mater.* **2003**, *15* (19), 1595−1598.
(43) Leopold, N.; Lendl, B. A new method for fast preparation of highly surface-enhanced Raman scattering (SERS) active silver colloids at room temperature by reduction of silver nitrate with hydroxylamine hydrochloride. *J. Phys. Chem. B* **2003**, *107*, 5723−5727.
(44) Akinoglu, E. M.; Morfa, A. J.; Giersig, M. Understanding anisotropic plasma etching of two-dimensional polystyrene opals for advanced materials fabrication. *Langmuir* **2014**, *30*, 12354−12361.
(45) Kim, S.; Joo, J.-H.; Kim, W.; Bang, A.; Choi, H. W.; Moon, S. W.; Choi, S. A facile, portable surface-enhanced Raman spectroscopy sensing platform for on-site chemometrics of toxic chemicals. *Sens. Actuators, B* **2021**, *343*, 130102.

https://doi.org/10.1021/acsomega.3c07167
ACS Omega 2023, 8, 47146−47152